THE ASTROPHYSICAL JOURNAL, 467:L121–L124, 1996 August 20

He I 10830 Å WING ASYMMETRY IN POLAR CORONAL HOLES: EVIDENCE FOR RADIAL OUTFLOWS

A. K. DUPREE
Harvard-Smithsonian Center for Astrophysics, 60 Garden Street, Cambridge, MA 02138
M. J. PENN
National Solar Observatory, National Optical Astronomy Observatories,[1] P.O. Box 26732, Tucson, AZ 85726-6732
AND
H. P. JONES
NASA/GSFC, Laboratory for Astronomy and Solar Physics, Greenbelt, MD 20771
Received 1996 May 16; accepted 1996 June 5

ABSTRACT

Imaging spectroscopy of the Sun, carried out across the the solar poles, yielded several thousand profiles of the He I 10830 Å chromospheric absorption line with effective spatial pixels of 1.1×2 arcsec^2. Profiles of He I 10830 Å show the relative blue-wing absorption is stronger in the coronal holes than in the quiet Sun, creating an asymmetric profile indicative of mass outflow. Within the coronal holes, blueshifted line wings are found where He I absorption is weak, corresponding to the center of supergranular cells. However, in the quiet Sun, there is no line wing shift in supergranular centers. Spatially compact regions of strong red-wing absorption also occur across the disk. Within the polar coronal holes, the amplitude of the wing shift shows a linear dependence with cos θ (where the angle θ is measured with respect to an outward normal to the Sun's surface), suggesting that a radial outflow occurs with a characteristic speed of $\sim$8 km s^{-1}. These observations represent the first detection of systematic outflows near the chromosphere transition region interface that appear to mark the origin of the high-speed wind acceleration from the solar surface.

Subject headings: Sun: chromosphere — Sun: corona — Sun: infrared — solar wind — stars: mass loss

1. INTRODUCTION

Identification of the source of the mass flux of the solar wind in the Sun's atmosphere remains a fundamental challenge to solar physics. Space experiments demonstrate that the high-speed wind originates from coronal holes located at the solar poles and on the disk; the high-speed wind is the basic equilibrium form of the solar wind (Bame et al. 1977) that dominates the heliosphere at solar minimum. Measurements above a coronal hole suggest the flow speed attains 200 km s^{-1} at 2 $R_\odot$ (Strachan et al. 1993). Theoretical models also yield supersonic flows at 2–3 $R_\odot$ (Esser & Habbal 1996; McKenzie, Banaszkiewicz, & Axford 1995). Acceleration of the polar wind is almost complete by 10 $R_\odot$ (Grall et al. 1996). Both the site of the wind's origin in the solar atmosphere as well as its acceleration profile are unknown. While the reduced intensity of coronal emission in the holes is well documented and reflects their lower densities and temperatures (Withbroe & Noyes 1977), it is puzzling that no firm dynamic signature of the solar wind has been found in the solar atmosphere itself.

Rocket observations (Rottman, Orrall, & Klimchuk 1982), with effective resolution of $\approx 1'$ across a coronal hole on the disk, detected a wavelength shift in a coronal and transition region line corresponding to an outflow velocity of 12 km s^{-1} for Mg X (625 Å) and 7 km s^{-1} for O V (629 Å). Yet *Skylab* spectra of a coronal hole on the disk (Doschek, Feldman, & Bohlin 1976) showed no velocity shift of O V (1218 Å). Reanalysis suggests that both measurements are consistent with a static atmosphere (Brekke 1993; Dere 1994). The NRL High Resolution Telescope and Spectrograph (HRTS) observed C IV in a coronal hole on the solar disk (Dere et al. 1989) with a spatial resolution of $\approx 2''$ and concluded downflows were present, although a greater proportion of outflows occurred in the hole (26%) as compared to the quiet Sun (7%). Many of the earlier studies represent averages over relatively large areas on the Sun that would dilute small-scale velocity structures. Moreover, most of the measured transitions are resonance lines and subject to optical depth effects that can compromise the interpretation of a wavelength shift. Emission in a resonance transition is susceptible to self-absorption on the short-wavelength side of a line profile, creating apparent redshifts in an outwardly accelerating atmosphere.

To study the chromospheric velocity field, spectra of the He I 10830 Å transition in solar coronal holes and the quiet Sun were obtained with good spatial resolution and wide field of view. Because He I absorption is weaker in coronal holes than in other solar features, the equivalent width has become a common diagnostic of the presence of coronal holes as observed in full-disk 10830 Å spectroheliograms (Harvey et al. 1975). However, the He I 10830 Å transition is also particularly well suited for detection of chromospheric dynamics (Dupree, Sasselov, & Lester 1992a). Indeed, the profiles of the He I 10830 Å line in luminous cool stars reveal supersonic outflow occurring in the chromosphere (Dupree et al. 1992a; Dupree, Whitney, & Avrett 1992b), and this motivated our study of the profiles in the Sun. In semiempirical solar models (Avrett, Fontenla, & Loeser 1994; Jones, Harvey, & Andretta 1994), He I 10830 Å is formed higher in the solar atmosphere than the Hα and Ca II K cores in optically and geometrically thin domains well separated from the photosphere and lower chromosphere (Avrett & Loeser 1992). The strength of the He I 10830 Å absorption couples indirectly to local thermody-

[1] Operated by the Association of Universities for Research in Astronomy, Inc. (AURA) under cooperative agreement with the National Science Foundation.

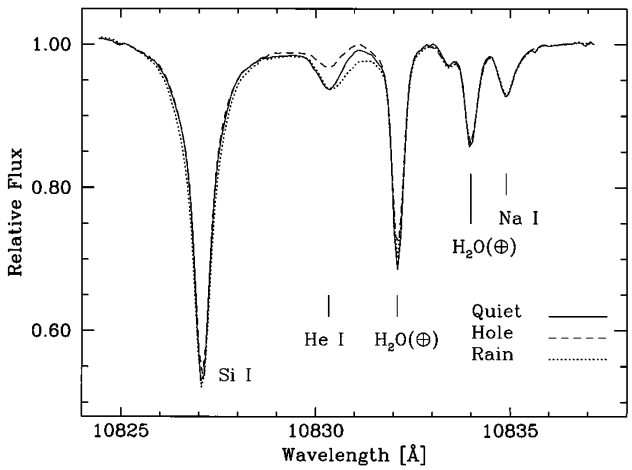

FIG. 1.—Sample spectra. The raw spectra have been normalized with a fit to the continuum, shifted to a photospheric wavelength scale, and spectra from many spatial positions have been averaged to produce three sample spectra: the quiet Sun, a coronal hole, and downflow regions, here labeled "rain." The spectra are virtually indistinguishable except for the He I 10830 Å feature.

namic conditions since the source function for the line is due almost entirely to scattering of photospheric radiation, and the ionization equilibrium is strongly influenced by photoionizing EUV and soft X-ray radiation from external coronal and transition region sources. He I 10830 Å is not a resonance transition, so optical depths are small. Thus, the spectral shape of the line is almost entirely determined by local flows near the base of the transition region; this differs from the cores of the resonance lines of Mg II and Ca II, which are formed in the low chromosphere and respond to thermodynamic transients through their collisionally dominated source functions.

2. OBSERVATIONS

Observations were obtained with the National Solar Observatory Kitt Peak Vacuum Tower telescope on 1995 October 17 and November 9 using the NASA/NSO spectromagnetograph (Jones et al. 1992). The spectral dispersion of the observations, 0.084 Å pixel^{-1}, corresponds to a resolution of $\lambda/\Delta\lambda = 64{,}000$ for 2 pixel sampling; the 150 pixel spectra covered a spectral range of 12.6 Å, roughly centered on 10830 Å. The spatial dispersion along the spectrograph slit is 1.″14 pixel^{-1}, but for improved spectra, the scanning rate and frame integration were modified to produce a step size of 2.″0, resulting in rectangular pixels in the image plane. The field of view of 452 slit pixels by 750 slit steps provides about 10^5 spectra with effective spatial pixels 1.14×2 arcsec^2 each, covering a total area of $515'' \times 1500''$ on the Sun. Effective dwell times were about 1.8 s per slit position. The data were collected as part of another program to study the height of the He I 10830 Å emission shell above the solar limb; details of that program, along with a discussion of the data reduction, can be found in Penn & Jones (1996).

Averaged spectra from different spatial regions are shown in Figure 1. Pixels corresponding to a polar coronal hole were first selected using maps of the spectrally integrated He I absorption for solar latitude greater than |62°|. For these pixels, the radius vector from solar center r was confined to the range, $r/R_\odot$ equal to 0.92–0.95. As discussed below, using wing shift maps, about one-half of the originally selected pixels were retained resulting in the averaging of 600 spectra. Pixels associated with quiet-Sun regions were identified as those pixels outside of the polar coronal hole at solar latitude less than |55°| and between a radius vector range of 0.92–0.95; 9000 spectra were averaged to produce the quiet-Sun spectrum. The third spectrum in Figure 1 has been summed over downflow regions using 900 spectra. These pixels were selected from the wing shift maps discussed below and were taken from radius vectors from 0.50 to 0.95.

For each spectrum, spectral pixels in the blue wing of the Si I line (about 10825.0–10825.5 Å) and pixels redward of the telluric lines (about 10836.0–10836.5 Å) were fitted with a linear function; no spectral pixels from 10825.5 to 10836.0 Å were used to compute continuum parameters. A continuum defined in this way was fitted to each spectrum before averaging. This function provides a good continuum fit at the long-wavelength end, but Figure 1 shows that a systematic error is present in the continuum fit of about 1% at the short-wavelength end. This introduces a systematic effect in further reduction, but the effect is equivalent at all spatial pixels. The continuum fitting provides equally good fits in all the spatial regions discussed. After averaging, the spectra were aligned based on the laboratory wavelengths of the photospheric Si I, Na I features (p-modes should be negligible with this spatial averaging that includes 600–9000 spectra) and the telluric lines. The strong He I line, comprising the blended members of the multiplet at 10830.250 and 10830.341 Å, is clearly visible. The weakest component of the multiplet at 10829.081 Å is not apparent, since the optical depth of this transition causes measurable effects only in filaments, plages, and flares (see Harvey & Livingston 1994; Penn & Kuhn 1995). The He I 10830.3 Å line profiles alone change dramatically among the three spectra.

A technique to characterize the line wings was developed following the standard centroid method (i.e., Gurman 1987), except the centroids of the line wing and the line core were computed separately. Such methods, a variant of a line bisector, are frequently used to detect subtle structures and velocity shifts in moving stellar atmospheres (Dravins 1982). Three intensity thresholds relative to the line center depth were established to define the line wing ($I_{\rm wing} = 0.35$, 0.40, and 0.45 times the line depth) and the line core ($I_{\rm core} = 0.80$, 0.85, and 0.90 times the line depth). The exact wavelengths of the intersections of these intensity thresholds with the line profiles ($\lambda_{\rm wing}$ and $\lambda_{\rm core}$) were computed with a cubic interpolation or, if this was not possible, with a simple linear interpolation. In regions of weak He I absorption, noise prevents the calculation of these intensity threshold wavelengths; of the total 2.7×10^5 solar spectra collected, 1.6×10^5 spectra had a sufficient signal-to-noise ratio to compute at least two intensity threshold wavelengths in both the line wing and line core. The centroid wavelength was computed for the line wing with $\lambda^C_{\rm wing} = (\Sigma_{\rm wing} \lambda_{\rm wing} I_{\rm wing})/(\Sigma_{\rm wing} I_{\rm wing})$ and similarly for the line core. Finally, the wing shift parameter is defined as the line wing centroid wavelength minus the line core centroid wavelength, $\lambda^C_{\rm wing} - \lambda^C_{\rm core}$.

The wing shift parameter is a differential measurement, and many subtle systematics are removed from the data. The most pronounced benefit is the removal of large-scale gradients seen in the line center position maps; scattered light is well known as a source of error in line center position calculations, and its effects are visible in maps of the line center position. The differential nature of the wing shift computation removes the scattered light systematics. Although the wing shift param-

eter is expressed in velocity units, the detailed interpretation of this velocity must rely on full profile calculations with realistic models.

3. RESULTS

A map of the spectrally integrated He I 10830 Å line absorption and a map of the wing shift parameter were constructed to identify the spatial distribution of the line profiles from the south pole observations of 1995 October (Fig. 2 [Pl. L13]). The most noteworthy feature in the wing shift map is a dark region at the south pole, signifying a region of a blueshifted He I wing. This region corresponds to the southern polar coronal hole, the extent of which can be roughly outlined using the map of spectrally integrated He I absorption (where the integration was performed over ±1.1 Å from line center). About half of all the spatial pixels within the boundaries of the coronal hole show wing shifts to short wavelengths; regions with low He I absorption (bright regions in Fig. 2*a* corresponding to supergranule centers) show more wing shift, whereas regions with stronger He I absorption (dark regions in Fig. 2*a*, the network) show little wing shift. The network areas with stronger He I absorption both inside and outside coronal holes usually show no wing shift. Spatially compact redshift areas ("rain"), which appear as bright points, are scattered across the midlatitudes in the wing shift image (Fig. 2*b*). The map of the wing shift parameter from data taken on 1995 November 9 of the northern polar coronal hole, although not displayed here, shows similar features.

It is important to note that the emission above the limb shows no systematic wing shift as is observed on the disk, confirming that a 10829 Å He I component does not disturb the line wing measurement. The spectral widths of both He I components are larger in the emission shell than on the disk (Penn & Jones 1996), suggesting that contamination from the blue He I component would be more pronounced in the emission shell. However, no such contamination is seen.

Examination of the wing shift map in Figure 2 suggests that within the coronal hole, there is a center-to-limb variation of the wing shift. The center-to-limb behavior is shown in Figure 3 for radially averaged wing shifts from the coronal hole, the quiet Sun, and downflow regions ("rain") from the 1995 October 17 data. The angle θ is measured from the solar vertical, and thus cos $\theta = 0$ is the solar limb and cos $\theta = 1$ is the center of the solar disk. The quiet-Sun wing shifts, although relatively constant with cos θ, are systematically offset from zero velocity. This is likely to be contamination from the strong wings of the Si I line; the red wing of the Si I line adds a slope to the He I line that is not corrected, and thus the He I line wing is systematically shifted blueward of the He I line core. (It is also possible that the unequal strengths of the blended 10830.25 and 10830.34 Å components contribute to this shift or that it represents a real flow, but data with a wider spectral window, better continuum fitting, and Si I line subtraction are needed to address this issue properly.) The coronal hole wing blueshifts show a strong linear dependence with cos θ. A linear fit reveals two interesting features: first, the intercept of this fit at cos $\theta = 0$ agrees with the quiet-Sun wing shift. This again implies that the quiet-Sun blueshift is a systematic effect caused by the Si I line and shows that the coronal hole spectra suffer equally from this systematic error.

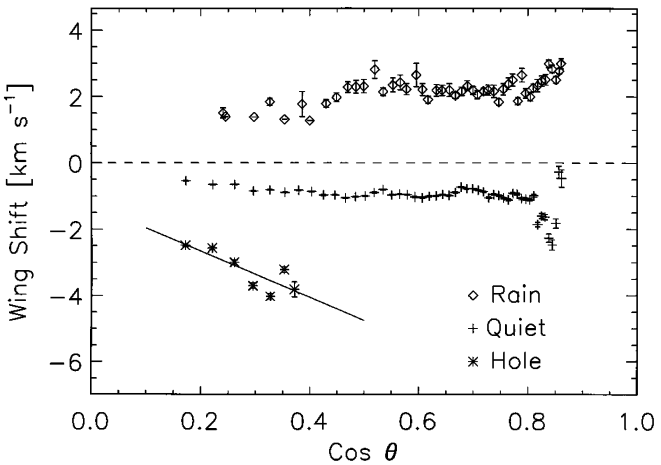

FIG. 3.—Center-to-limb behavior of the observed wing shifts. Plotted are the mean wing shifts seen in the quiet Sun (*plus signs*), mean wing shifts seen in the coronal hole (*asterisks*), and the mean wing shifts seen in downflow regions, "rain" (*squares*) with respect to cos θ. (Cos $\theta = 1$ at disk center.) Error bars (many are smaller than the symbols) are the standard deviation of the mean (1 σ) for the radial binning. The polar coronal hole does not extend to low latitudes. The coronal hole wing shifts show the strongest center-to-limb dependence (solid line marks a linear regression fit), suggesting a radial flow with a characteristic speed of -7.0 ± 2.1 km s^{-1}.

Second, the slope of the coronal hole wing shifts implies a radial outflow velocity of 7.0 ± 2.1 (1 σ) km s^{-1}, since $v_{\rm obs} \propto v_{\rm rad}$ cos θ. A fit to the radial dependence of the coronal hole wing shifts from the 1995 November 9 measurements of the northern polar coronal hole implies a radial outflow velocity of 9.1 ± 0.9 (1 σ) km s^{-1}. Thus, the radial dependence of wing shift measurements from both polar holes reveals a systematic outflow of about 8 km s^{-1}. This value is a lower limit to the flow because it is measured near the midpoint of the line profile; the short-wavelength extent of the profile can map faster outflow velocities higher in the atmosphere since the line is optically thin.

The downflow ("rain") regions (Fig. 3, *upper curve*) show mean amplitudes of about 2 km s^{-1} with no strong dependence on cos θ, which suggests that the associated flows occur with a variety of inclination angles. The lower amplitude toward the limb (cos $\theta < 0.45$) shown in Figure 3 for 1995 October 19 is in harmony with a preference toward radially oriented downflows, but a similar trend is not evident in the 1995 November 9 data. More observations are needed to establish the center-to-limb variation of these features.

4. DISCUSSION

The blueshift occurs predominantly in He I–weak absorption regions, which can be identified as the center of supergranular cells by comparison of the He I absorption with the wing shift maps (see Fig. 2).

Can this observed outflow account for the fast solar wind? The contribution of the outflowing He I material to the solar wind can be estimated as follows. The mass flux from a coronal hole, $F_{\rm hole}$ (protons cm^{-2} s^{-1}), is given by the equation of continuity: $F_{\rm hole} = f \times n \times v = 5.6 \times 10^{14}$, where f is the filling factor of the outflowing regions in the coronal hole area (here taken as 0.5 based on our observations), n is the proton

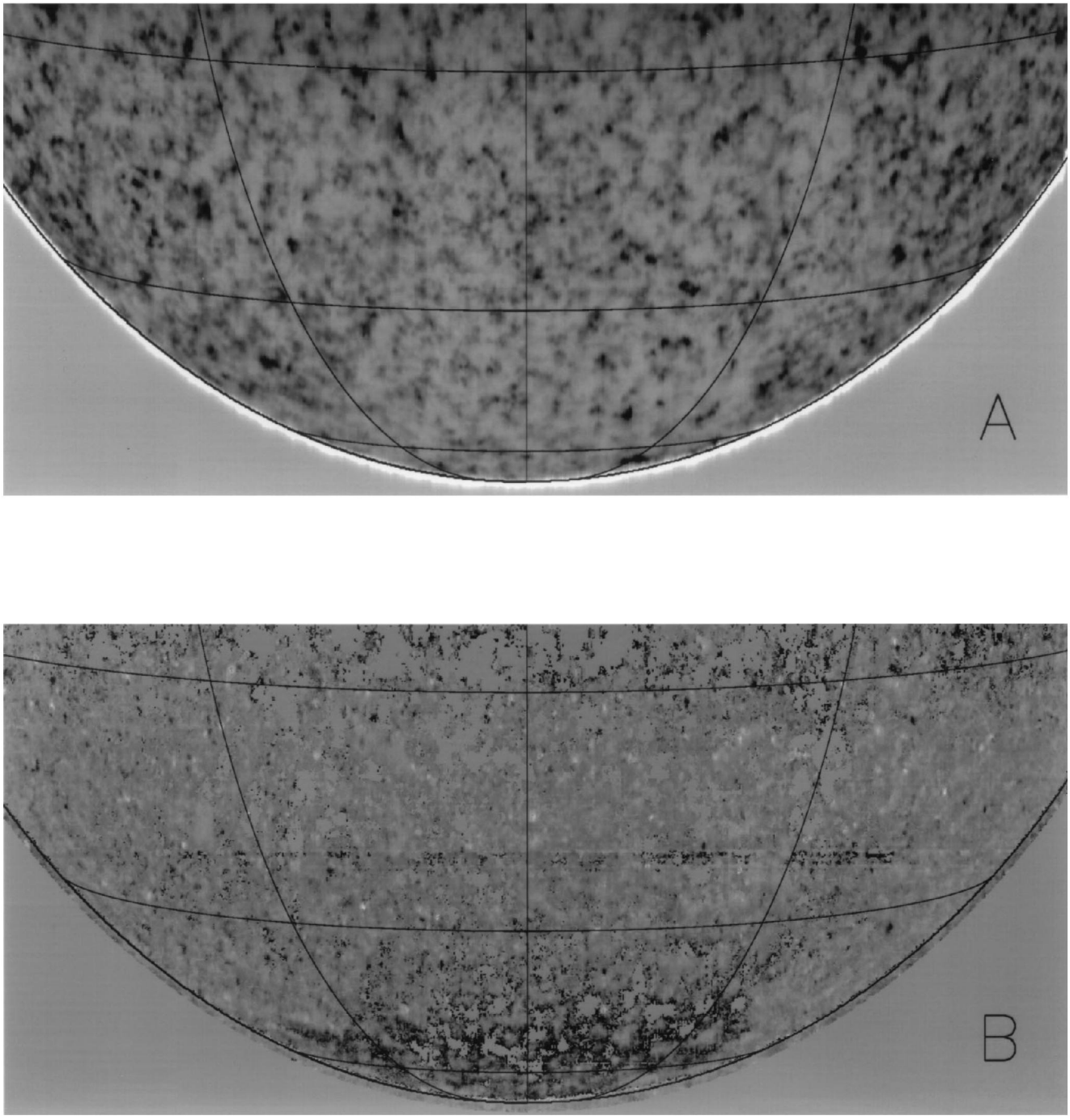

FIG. 2.—Map of (*a*) the spectrally integrated He I line absorption and (*b*) the wing shift parameter from the 1995 October 17 observation of the south pole. Solar coordinates are overlaid with latitude lines at 30°, 50°, and 70°. The He I line absorption is dark where there is maximum absorption and light where minimum absorption occurs. The wing shift image shows blue shifts as dark regions. Spatially compact redshift areas appear as white points in the lower figure, scattered across the wing shift image. Two instrumental effects are present in Fig. 2*b*: a "strip" at latitude −45° and large areas near the edge of the field of view below |30°| where the signal is weak.

DUPREE, PENN, & JONES (see 467, L123)

density (a value of 1.4×10^9 cm^{-3} is selected[2]), and v assumed as 8 km s^{-1} from the extrapolation of our measurement to radial flow. The fast solar wind is measured by *Ulysses* (Phillips et al. 1995) to have a velocity of 750 km s^{-1} and a proton density of 3 cm^{-3} when scaled to a distance of 1 AU. Thus, for a filling factor of 0.8 (McKenzie et al. 1995), the mass flux in the fast solar wind at 1 AU, $F_{1\,\mathrm{AU}}$, equals 1.8×10^8 protons cm^{-2} s^{-1}. The fraction of the Sun's area needed to produce all of this observed flux is given by $(F_{1\,\mathrm{AU}}/F_{\mathrm{hole}}) \times (d/R_\odot)^2 \approx 1.4\%$, where d equals the mean Sun-Earth distance, and $R_\odot$ is the solar radius. This fraction is less than the measurement (Bohlin 1977) that 15% of the solar surface was covered by polar coronal holes (north and south) during its 1973–1974 solar minimum and indicates that the measured outflow mass flux could easily provide sufficient material to form the fast solar wind.

Significant downflows are not observed in the coronal holes, implying that the observed wing shift is not associated with a local circulation flow. The outflows occur at the center of the supergranulation cells. Since coronal polar plumes may be associated with coronal bright points in the supergranulation network (Habbal 1992), the plumes would not appear to be the source of the wind. The most straightforward interpretation of these observations suggests that the helium outflows mark the onset of acceleration of the fast solar wind. Such a substantial mass flow through a temperature gradient can have profound effects on the ionization equilibrium and energy balance in the transition region and corona (Dupree, Moore, & Shapiro 1979) as well as on traditional density diagnostics (Raymond & Dupree 1978).

We can not identify the small redshifted areas, termed "rain," that are scattered across the disk. The "rain" regions usually lack nearby upflows, suggesting that these are not siphon flows. The redshifted areas are most prominent at midlatitudes and appear associated with both strong and weak He I features—the network and cell centers. Jetlike features in the C I lines were discovered with both red- and blueshifts in network cell centers with resolution of ≈1″ (Dere, Bartoe, & Brueckner 1983). Episodic heating of the corona could initiate downflows because of propagating acoustic waves (Hansteen 1993) or lead to simple gravitational downfall of cooling material (Kopp & Poletto 1991). Time-dependent calculations may be necessary to understand the helium excitation observed in downflows.

Clearly, the occurrence of a coronal hole on the disk, which is likely during this time of solar minimum, should be observed with the He I spectromagnetograph and, hopefully, in conjunction with the spectroscopic instruments on the recently launched *SOHO* satellite in order to map the flow at different atmospheric levels.

[2] Hydrostatic models of a quiet-Sun cell center, FAL-A (Fontenla, Avrett, & Loeser 1993) suggest $n = 1.6 \times 10^{10}$ cm^{-3} for $h = 2000$ km. This height approximates the observed limb height of the He I emission. Outflowing material forming the short-wavelength side of the He I line in a coronal hole lies above 2000 km. Because the heights of the Lyman continuum and the C II line in a polar hole are higher by 1000–1300 km than in the quiet Sun (Huber et al. 1974), we select a density corresponding to 2300 km in the cell center model (FAL-A), 2.8×10^9 cm^{-3} and lower this value by a factor of 2 to account for the lower chromospheric pressure in the hole (Vernazza & Noyes 1972).

Discussions with R. Esser have been especially helpful. Research conducted at the National Solar Observatory is made possible through a cooperative agreement with the National Science Foundation. NSO/Kitt Peak data used here are produced cooperatively by NSF/NOAO, NASA/GSFC, and NOAA/SEL. Partial funding was provided through NASA Space Physics Supporting Research and Technology tasks 170-38-52-14 and 170-38-52-19. M. Penn is supported by *SOHO* and NASA/GSFC.

REFERENCES

Avrett, E. H., Fontenla, J. M., & Loeser, R. 1994, in IAU Symp. 154, Infrared Solar Physics, ed. D. M. Rabin, J. T. Jefferies, & C. Lindsey (Dordrecht: Kluwer), 35
Avrett, E. H., & Loeser, R. 1992, in ASP Conf. Proc. 26, 7th Cambridge Workshop on Cool Stars, Stellar Systems, and the Sun, ed. M. Giampapa & J. Bookbinder (San Francisco: ASP), 489
Bame, S. J., Asbridge, J. R., Feldman, W. C., & Gosling, J. T. 1977, J. Geophys. Res., 82, 1487
Bohlin, J. D. 1977, Sol. Phys., 51, 377
Brekke, P. 1993, ApJ, 408, 735
Dere, K. P. 1994, Space Sci. Rev., 70, 21
Dere, K. P., Bartoe, J.-D., & Brueckner, G. E. 1983, ApJ, 267, L65
Dere, K. P., Bartoe, J.-D., F., Brueckner, G. E., & Recely, F. 1989, ApJ, 345, L95
Doschek, G. A., Feldman, U., & Bohlin, J. D. 1976, ApJ, 205, L177
Dravins, D. 1982, ARA&A, 20, 61
Dupree, A. K., Moore, R. T., & Shapiro, P. R. 1979, ApJ, 229, L101
Dupree, A. K., Sasselov, D. D., & Lester, J. B. 1992a, ApJ, 387, L85
Dupree, A. K., Whitney, B. A., & Avrett, E. H. 1992b, in ASP Conf. Proc. 26, 7th Cambridge Workshop on Cool Stars, Stellar Systems, and the Sun, ed. M. Giampapa & J. Bookbinder (San Francisco: ASP), 525
Esser, R., & Habbal, S. R. 1996, in Proc. Solar Wind Eight, ed. D. Winterhalter, J. Gosling, S. R. Habbal, W. Kurth, & M. Neugebauer (New York: AIP), in press
Fontenla, J. M., Avrett, E. H., & Loeser, R. 1993, ApJ, 406, 319
Grall, R. W., Coles, W. A., Klinglesmith, M. T., Breen, A. R., Williams, P. J. S., Markkanen, J., & Esser, R. 1996, Nature, 379, 429
Gurman, J. B. 1987, Sol. Phys., 108, 61
Habbal, S. R. 1992, Ann. Geophys., 10, 34
Hansteen, V. 1993, ApJ, 402, 741
Harvey, J. W., Krieger, A. S., Timothy, A. F., & Vaiana, G. S. 1975, Osserv. Mem. Oss. Astrofis. Arcetri, 104, 50
Harvey, J. W., & Livingston, W. C. 1994, in IAU Symp. 154, Infrared Solar Physics, ed. D. M. Rabin, J. T. Jefferies, & C. Lindsey (Dordrecht: Kluwer), 59
Huber, M. C. E., et al. 1974, ApJ, 194, L115
Jones, H. P., Duvall, T. L., Jr., Harvey, J. W., Mahaffey, C. T., Schwitters, J. D., & Simmons, J. E. 1992, Sol. Phys., 139, 211
Jones, H. P., Harvey, J. W., & Andretta, V. 1994, in Proc. 3rd *SOHO* Workshop, Solar Dynamic Phenomena & Solar Wind Consequences, ed. J. Hunt (ESA SP-373), 345
Kopp, R. A., & Poletto, G. 1991, in Mechanisms of Chromospheric and Coronal Heating, ed. P. Ulmschneider, E. R. Priest, & R. Rosner (New York: Springer), 634
McKenzie, J. F., Banaszkiewicz, M., & Axford, W. I. 1995, A&A, 303, L45
Penn, M. J., & Jones, H. P. 1996, Sol. Phys., in press
Penn, M. J., & Kuhn, J. P. 1995, ApJ, 441, L51
Phillips, J. L., et al. 1995, Science, 268, 1030
Raymond, J. C., & Dupree, A. K. 1978, ApJ, 222, 379
Rottman, G. J., Orrall, F. Q., & Klimchuk, J. A. 1982, ApJ, 260, 32
Strachan, L., Kohl, J. L., Weiser, H., Withbroe, G. L., & Munro, R. H. 1993, ApJ, 412, 410
Vernazza, J. E., & Noyes, R. W. 1972, Sol. Phys., 26, 335
Withbroe, G. L., & Noyes, R. W. 1977, ARA&A, 15, 363